HHS Public Access

Author manuscript

Cell Rep. Author manuscript; available in PMC 2025 May 29.

Published in final edited form as:

Cell Rep. 2023 March 28; 42(3): 112176. doi:10.1016/j.celrep.2023.112176.

Multi-finger receptive field properties in primary somatosensory cortex: A revised account of the spatiotemporal integration functions of area 3b

Natalie K. Trzcinski[4], **Steven S. Hsiao**[1,2], **Charles E. Connor**[1,2], **Manuel Gomez-Ramirez**[3,5,*]

[1]The Zanvyl Krieger Mind/Brain Institute, The Johns Hopkins University, Baltimore, MD 21218, USA

[2]The Solomon H. Snyder Department of Neuroscience, The Johns Hopkins School of Medicine, Baltimore, MD 21218, USA

[3]Department of Brain and Cognitive Sciences, University of Rochester, Rochester, NY 14642, USA

[4]National Institute of Neurological Disorders & Stroke, National Institutes of Health, Bethesda, MD, USA

[5]Lead contact

SUMMARY

The leading view in the somatosensory system indicates that area 3b serves as a cortical relay site that primarily encodes (cutaneous) tactile features limited to individual digits. Our recent work argues against this model by showing that area 3b cells can integrate both cutaneous and proprioceptive information from the hand. Here, we further test the validity of this model by studying multi-digit (MD) integration properties in area 3b. In contrast to the prevailing view, we show that most cells in area 3b have a receptive field (RF) that extends to multiple digits, with the size of the RF (i.e., the number of responsive digits) increasing across time. Further, we show that MD cells' orientation angle preference is highly correlated across digits. Taken together, these data show that area 3b plays a larger role in generating neural representations of tactile objects, as opposed to just being a ''feature detector'' relay site.

Graphical abstract

*Correspondence: mgomezra@ur.rochester.edu.

AUTHOR CONTRIBUTIONS

Conceived and designed the experiments: N.K.T., S.S.H., C.E.C., and M.G.R. Performed the experiments: N.K.T. and M.G.R. Analyzed the data: N.K.T. and M.G.R. Wrote the paper: N.K.T. and M.G.R.

SUPPLEMENTAL INFORMATION

Supplemental information can be found online at https://doi.org/10.1016/j.celrep.2023.112176.

DECLARATION OF INTERESTS

The authors declare no competing interests. This article was prepared while N.K.T. was employed at Johns Hopkins University. The opinions expressed in this article are those of the authors and do not reflect the view of National Institutes of Health, the Department of Health and Human Services, or the United States Government.

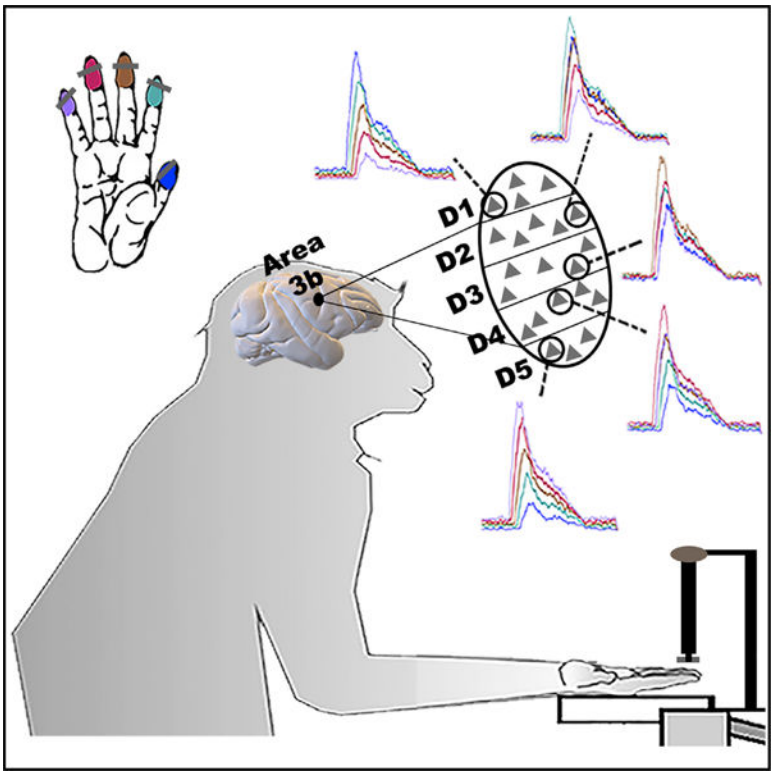

In brief

Trzcinski et al. show that area 3b cells have receptive fields (RFs) that span multiple fingers, a finding that runs counter to the leading RF model in somatosensory neocortex. The emergence of multi-fingers RFs is driven by feedback mechanisms, with cells' cross-finger orientation preference phase-shifted to optimally encode curved objects.

INTRODUCTION

Object sensing and manipulation (i.e., haptics) is largely mediated by brain mechanisms that integrate tactile information across fingers. Haptics commences in the periphery with specialized cells that transduce objects' physical features into neural signals that are relayed and combined in the brain.[1–3] As information is relayed to the brain, the receptive field (RF) of cells increases and becomes more elaborate. Peripheral cells with the highest spatial acuity (i.e., Merkel cells) are confined to small skin areas (2–8 mm), whereas RFs in area 3b have been thought to be a single finger,[4–7] although plasticity can modulate cells' RF size in area 3b.[8,9] In cortical areas down-stream of area 3b, RFs tend to encompass multiple fingers (e.g., area 1) or the whole hand (e.g., area 2 and secondary somatosensory cortex; SII) and have complex inhibitory and excitatory spatiotemporal properties.[10–13] Cells in area 3b, and to a lesser extent area 1, are thought to operate as ''local feature detectors,'' with RFs akin to those of simple cells in primary visual cortex.[14] These observations have led to the view that tactile object perception emerges across cortical stages, likely in area 2 or beyond, with area 3b serving as a cortical relay site that encodes tactile features confined to individual digits.[1]

Our understanding of area 3b cells' RF size is largely derived from anesthetized and awake-behaving studies in non-human primates that primarily analyzed responses to stimulation on a single finger.[4,5,10,11,14–22] For many of these studies, the goal for each recording site was to define the smallest RF where light tactile stimulation elicited a clear and robust response. Typically, researchers localized the finger with the maximum response (i.e., the preferred finger) using handheld probes and then used motorized devices to systematically stimulate the preferred finger only. Further, recordings were commonly performed in layer IV of SI, which contains cells with the smallest RF boundaries. These non-human primate studies (both anesthetized and awake-behaving preparations) generated findings that were highly consistent.[5,20,23] Namely, cells in area 3b had RFs limited to a single digit, whereas adjacent areas had cells with RFs that extended to multiple digits, and sometimes the whole hand. These early studies paved the way for research to go beyond early concepts of SI, as a single area, to our current understanding of areas 3a, 3b, 1, and 2 as separate representations. Although much was learned from these studies, the concern with their mapping and experimental approach is that we may have an incomplete understanding of the cross-finger integration properties of area 3b cells. Supporting this concern, we used automatized stimulators to show that area 3b cells integrate inputs from proprioceptive and cutaneous modalities,[24] a finding that runs counter to the modality specificity model of the somatosensory system.[2,20,25] Thus, there is a need to comprehensively characterize area 3b[0]s RFs using automated and systematic approaches.

There have only been a few studies that recorded activity in area 3b while stimulating multiple locations on the hand using reliable motorized tools.[26] Co-stimulation of the preferred skin region and a neighboring site modulated responses relative to stimulation on the preferred skin region alone, suggesting that area 3b cells have multi-digit (MD) non-classical RFs. However, this study failed to systematically test responses across all digits and collapsed across single- and multi-unit spiking data. Many cells reported in Reed and colleagues[26] were observed in boundary locations of the digit representations. Therefore, it is unclear how many cells classified with an MD RF truly emanate from an individual cell or multiple cells. Similar concerns are raised for a recent non-human primate study, which also reported MD RF cells in area 3b.[27] That said, the studies by Reed and colleagues[26] and Lazar and colleagues[27] provide evidence that cells in area 3b have more complex cross-finger integrative properties than previously thought. However, the mechanisms that give rise to these MD RFs and how spatial information across fingers is represented by MD cells are still largely undetermined.

To address these questions, we performed single-unit recordings in the finger representation of area 3b while presenting oriented bars to different fingers in awake-behaving monkeys. Contrary to the prevailing model, we found that the majority of cells in area 3b have RFs that extend to multiple digits. MD RFs evolve as a function of time, suggesting that they are mediated by feedback mechanisms. We also found that MD cells tuned to oriented bars have an orientation preference across fingers that differs between 22.5° and 67.5°, an ideal range for encoding curved objects. Taken together, these data provide evidence that area 3b integrates sensory information across fingers, supporting the complex role of area 3b in mediating object representations in touch.

RESULTS

Two animals (*Macaca mulatta*) sat comfortably on a custom-made chair with their hands held supinated (Figure 1). We stimulated digits 2, 3, 4, or 5 while monkeys performed an unrelated visual contrast discrimination task. Tactile stimuli consisted of oriented bars (0°–157.5°, steps of 22.5°, indented 1 mm into the skin for 500-ms duration). Single-unit activity was recorded using a custom-built electrode microdrive with four linearly spaced electrodes from four hemispheres of the distal finger representation of area 3b (see STAR Methods section). We used similar functional mapping procedures as in previous studies[10,14,18,19,28,29] to ensure single-unit recordings were made in area 3b. Analyses were conducted in cells recorded >2 mm below the surface of the brain to avoid analyzing cells in area 1 (range = ~2 to ~5 mm past the estimated location of electrode contact with dura; note that estimation of electrophysiological recordings across cortical layers was not possible due to our recording approach). The anatomical organization of areas 1 and 3b in rhesus monkeys is highlighted by the inverse topography between the distal, middle, and proximal finger pad representation in areas 1 and 3b.[2] Recording from the proximal pad of area 3b may lead to the inclusion of area 1 cells with an RF over the proximal pad. As such, we only selected cells in area 3b with an RF over the distal finger pad.

Area 3b cells have RFs that cover multiple digits

The majority of area 3b cells (~57%) responded to stimulation on more than one digit, a finding that runs counter to simplified models of the somatosensory system based on minimal RF size.[4,5,23] Figure 2A shows examples of neurons with an RF over one (top row), two (second row), three (third row), or four (bottom row) digit(s). The insets in Figure 2A show averaged action potential waveforms recorded to each stimulated digit. Figure S1 shows additional examples of area 3b neurons with RFs over one, two, three, or four digits. Figure 2B shows the RF size distribution across the population. As expected, the proportion of cells in each RF size category decreased as a function of RF size, with ~43% of cells having an RF confined to a single finger, and ~10% of cells having an RF size that covered four digits. This pattern of effects was observed in each of the hemispheres recorded in both monkeys (Figure S2). A Kruskal-Wallis test showed that the firing rate of the preferred digit (i.e., the digit with the maximal response to the tactile stimulus) was significantly greater in neurons with larger RF size ($H[3473] = 83.19$, $p < 0.001$; Figure 2C). A regression test showed a systematic relationship between firing rate and RF size ($R^2 = .15$, $p < 0.001$). Similar findings were observed during the baseline firing rate ($H(3,473) = 19.56$, $p < 0.001$; Figure S3) and the firing rates to the second preferred digit ($H(2,269) = 46.03$, $p < 0.001$; Figure S4). The range in background firing rate here falls within the range reported in the literature.[24,26,30,31] The preferred digit location was uniformly distributed across all fingers, indicating that we equally sampled neurons from all finger representations of area 3b (Figure S5A; $X^2(3,473) = 0.57$, $p > 0.05$). Among cells with an MD RF, we found that the second most responsive digit was predominantly adjacent to the preferred digit (Figure S5B; $X^2(5,269) = 160.54$, $p < 0.001$).

The firing rate response in MD cells was not uniform across digits, indicating that MD cells have a digit that elicits a preferential response (i.e., a preferred digit; see Figure 3A). Figure

3A shows that a majority of MD cells (70%) had responses to the preferred digit that were significantly greater than those to the non-preferred digits ($X^2(2,269) = 35.60$, $p < 0.001$). We also found that differences in response magnitude between preferred and non-preferred digits increased as a function of RF size (Figure 3A orange, mustard, and green bars). Figure 3B shows the cumulative distribution of Fano factor (FF) to stimulation in the preferred digit location as a function of digit RF size. The data revealed higher FF in the preferred digit, a measure of neural response variability, across RF size condition ($X^2(3,464) = 35.60$, $p = 0.01$). A linear regression analysis showed a systematic shift in FF as a function of RF size, with larger FF in cells with a larger digit RF size ($R^2 = 0.03$; $p < 0.01$). Increases in RF_{FF} are likely due to increased response variability across fingers (i.e., cells having non-homogeneous response functions across responsive digits) since the spiking of cells (i.e., $\hat{R}$) increased as a function of RF size (Figure 2C).

MD RF cells respond faster and have higher spike timing precision

Response latency to the preferred digit of MD cells was faster compared with that in cells with a single-digit (SD) RF ($X^2(1,476) = 24.65$, $p < 0.0001$). The upper panels in Figure 4A show examples of neural responses to stimulation on the preferred digit in cells with an SD (red trace, left y axes) and MD (blue trace, right y axes) RF. The lower panel in Figure 4A shows the cumulative distribution of onset time for the preferred digit on SD (red traces) and MD (blue traces) cells with excited (solid trace) and inhibited (dashed trace) initial responses, relative to baseline. As the figure shows, the earliest responses were primarily inhibited ($X^2(1,476) = 65.24$, $p < 0.0001$). Importantly, we only considered cells that had an initial response within 300 ms following stimulus onset. Somatosensory cortex has cells that respond only to the offset of the stimulus,[18,26,32,33] so including these cells in these analyses would introduce biases to the distribution. We found that ~69% of SD cells had an initial response that was excited (~31% of SD cells had an inhibited initial response). Similarly, ~60% of MD cells had an initial response that was excited (~40% of MD cells had an initial response that was inhibited).

The spike timing, measured as the coefficient of variation (CV) of the inter-spike interval (ISI),[34] was more regular in MD vs. SD cells ($Z = 5.69$; $p < 0.001$). Figure 4B shows the cumulative distribution of the CV of the ISI for SD (red trace) and MD (blue trace). The left inset of Figure 4B shows that the median CV of the ISI decreased as a function of RF size ($X^2(3,453) = 50.41$, $p < 0.0001$). As shown in the right inset of Figure 4B, cells with a significant response during the first 20 ms of stimulus onset exhibited more regular spiking if they had an MD vs. SD RF ($Z = 2.17$; $p < 0.05$). These data indicate that MD cells have more reliable feedforward inputs from first-order thalamic sources compared with cells with SD.

MD RFs in area 3b evolve across time

Response latencies to tactile stimulation in the non-preferred digits were systematically delayed, suggesting the MD RFs are generated by feedback (or reentrant) activity from downstream cortical sources. The upper panels in Figure 5 show examples of neural responses to tactile stimulation on each digit of a cell with an RF spanning four digits. The example cells show a systematic delay in response onset across finger stimulation. The

lower panel in Figure 5 shows the cumulative distribution of onset time for each responsive digit across MD cells. Onset response times were systematically delayed across responsive digits ($X^2(3,473) = 98.05$, $p < 0.0001$). The inset in the cumulative distribution of Figure 5 shows the median response onset time for each responsive digit across the population, with the fastest digit response occurring within the first 20 ms, the second fastest digit response occurring between 20 and 40 ms, and the remaining digit responses occurring after ~40 ms. A regression analysis showed a systematic relationship between response onset across stimulated fingers ($R^2 = 0.18$, $p < 0.0001$). Of note, response onset times in non-preferred digits were faster in digits that neighbored the preferred digit of the cell (Figure S6).

Orientation tuning properties decrease as RF size increases

Orientation tuning was more prevalent in the preferred digit of cells with an SD vs. MD RF ($X^2(3,215) = 124.93$, $p < 0.0001$). Figure 6A shows examples of orientation-tuned cells with an RF in one (upper left panel), two (upper right panel), three (lower left panel), or four (lower right panel) digits. The dashed black line shows the average product of the tuning functions between preferred and non-preferred digits. Figure 6B shows the percentage of orientation-tuned cells with a one-, two-, three-, or four-digit RF. With the exception of cells with a four-digit RF ($X^2(3.46) = 20.43$, $p < 0.001$), most MD cells with orientation tuning in the preferred digit also show significant orientation tuning in the non-preferred digits. Figure 6C shows the orientation index (OI) of cells with a one-, two-, three-, or four-digit RF. We observed greater orientation selectivity in SD vs. MD cells ($Z = 2.16$; $p < 0.05$). However, this difference was largely found between cells with a one- vs. three-digit RF (approaching significance; $Z = 1.89$; $p = 0.06$) and one- vs. four-digit RF ($Z = 2.42$; $p < 0.05$). We also failed to see significant differences in OI between digits ($H(3,458) = 2.83$, $p > 0.05$; Figure S7).

Orientation tuning preference of MD cells is correlated across digits

The preferred angle of preferred vs. non-preferred digits of MD cells is shifted between 22.5° and 67.5° ($R = 0.43$; $p < 0.05$; see black dashed lines in Figure 6A). Figure 6D (left panel) shows a polar plot of the difference in the preferred angle between preferred and non-preferred digits of orientation-tuned MD cells. The right panel of Figure 6D shows the percentage of cells with an angular difference between 0° and 90°. Most MD cells have a preferred angle difference between preferred and non-preferred digits of 22.5°, with the least preferred angle difference being 0° ($X^2(4,115) = 12.53$, $p < 0.05$).

DISCUSSION

Our study showed that the majority of cells in area 3b have an RF that spanned multiple digits, a finding that runs counter to the leading view of cells' RF size properties in the somatosensory system.[2,4–7] We also found that the firing rate response across each digit was heterogeneous in MD cells (indicating a preferred digit), with the firing rate disparity increasing with the RF size of cells. The relationship between firing rate and cells' RF size was also evident in the baseline activity of the preferred and second preferred digit, indicating common gain properties throughout the entire somatotopic RF of an MD cell. Taken together, these data suggest that response gain functions of area 3b cells are

dependent on their RF size, becoming more excitable, likely, by accumulating afferent synaptic activity from connected cells with similar somatotopic RFs.

The leading view in the somatosensory system indicates that area 3b predominantly operates as a ‘‘local feature detector,’’ relaying signals to downstream areas where cross-finger neural integration emerges.[1,3] Our data argue against this model by showing that a majority of area 3b cells have an RF that spans multiple digits. The question arises: why hasn’t this large incidence in MD RFs in area 3b been reported in the literature? We do not have a conclusive answer, but we suspect that standard practices in mapping somatosensory RFs play a large role. Most, if not all, studies have used handheld probes to initially map the classical RF properties of cells.[10,11,14,15,18,19,28,35] As we have shown, this approach can lead to an inaccurate view of the RF properties of neurons in the somatosensory system.[24] Using motorized devices, we demonstrated that neurons in areas 3a and 3b of SI (primary somatosensory cortex) integrate information from both cutaneous and proprioceptive channels, arguing against the modality specificity model of the somatosensory system.[2,20,25] Our findings are in agreement with more recent studies[26,27,36] and show that MD RFs of area 3b extend to classical RF structures, with cells’ excitation strength dependent on RF size. Our data argue in favor of using automated devices to systematically map cells’ RFs in the somatosensory system. This practice in mapping RFs will provide a detailed account of cells’ classical and non-classical RF properties, which can be used to generate more comprehensive models of haptics-related functions in the somatosensory system. Anesthetics is another potential factor driving the limited reports of MD RFs in area 3b, as many studies describing RF properties of area 3b were conducted under anesthetic preparations. Yet, anesthesia can have a significant impact on neurons’ activation strength,[37–39] so neural responses to non-preferred digit stimulation may have been substantially suppressed by the anesthetic. However, it is worth noting that a previous study indicated that anesthetics effects in somatosensory neocortex may be minimal in area 3b and more pronounced in associative areas.[5]

Temporal properties of the RF size in MD cells

Response latencies to tactile stimulation on the preferred digit were faster in MD vs. SD cells, with inhibited responses emerging at an earlier time point compared with excited responses. Timing differences between excited and inhibited activations may be driven by preferential projections from first-order thalamo-cortical (TC) neurons in the ventro-posterior nucleus of the thalamus. Although there is an approximate four-to-one excitatory/inhibitory cell ratio in cortex,[40] studies show that first-order TC cells project more strongly and with higher prevalence to inhibitory cells.[41–44] In support of this observation, TC excitatory currents in interneurons emerge fast, allowing inhibitory cells to fire spikes before feedforward inhibition emerges.[42] The same is not true for TC excitatory currents in pyramidal cells.[42] The implication of these data is that TC synapses drive interneurons much faster compared with excitatory cells. As such, in neocortical areas with a higher number of excitatory vs. inhibitory cells,[40] but where interneurons densely synapse onto local pyramidal cells (>50% within ~100 μm),[45] the population’s initial net response would be largely inhibited. This hypothesis fits well with our observation that inhibited responses were faster in area 3b cells. The finding that inhibited responses in MD cells have earlier

onset suggests that TC-projecting cells are preferentially biased toward area 3b cells with an RF across multiple digits, with these TC-projecting inputs driving area 3b cells with higher reliability compared with those of SD cells (Figure 4B).

A major finding of this paper is that the amount of digit responsivity of MD cells (i.e., the RF size of MD cells) increased as a function of time (Figure 5), with responses systematically delayed across non-preferred digits. This finding suggests that MD RFs are not generated by feedforward projections from TC relay cells but rather from neural sources that provide feedback to area 3b. Although we cannot ascertain the source that provides feedback to area 3b MD cells, a recent study in mice showed a direct and somatotopically aligned circuit between SI and SII.[46] This connectivity pattern has also been described in rats,[47] with first-order TC relay cells projecting in parallel and independently to SI and SII cortices. However, anatomical studies in non-human primates show that area 1 and SII have extensive feedback connections to the hand area representation of 3b.[48–50] Another strong possibility is that these MD RFs arise from feedback connections from area 3b cells that receive digit-specific input from first-order thalamic sources. Thus, it seems that MD RFs in area 3b may arise from a number of combinations of inputs from associative somatosensory areas and/or lateral connections between cells in different digit representations of area 3b. Clearly, further neuro-physiological studies are needed to identify the source(s) and laminar target(s) that generate these MD RFs in area 3b cells.

Orientation selectivity differs between SD and MD area 3b cells

The data revealed that orientation tuning was more prevalent in SD compared with MD cells (Figure 6B). SD cells also had increased orientation selectivity (Figure 6C), suggesting that cells with an SD RF have higher spatial acuity functions. These findings are consistent with human anecdotal and experimental observations showing that fine analyses of an object feature (e.g., textures, edges, pressure) are usually performed by scanning the surface with a limited number of fingers.[51] Of note, although studies in humans show that the distal finger pad of the index and middle fingers (i.e., D2 and D3) has the highest density of mechanoreceptors[52] and, thus, greater sensitivity, we failed to observe higher OI in cells with an RF over D2 or D3 (Figure S7).

Orientation preference across fingers was correlated in MD cells but largely phase-shifted between 22.5° and 67.5°, with the most common difference at 22.5° (Figure 6D). This cross-finger orientation angle disparity is different than the cross-finger angle preference in SII cortex,[53] wherein cells' orientation preference is highly similar across responsive finger pads (i.e., angle disparity between fingers ~0°). These cross-finger coding discrepancies could arise from neural transformations between area 3b and SII. Although there are direct connections between area 3b and SII,[54,55] there is at least one synapse between down-stream outputs of area 3b to SII (e.g., area 3b → area 1 → SII). Orientation selective populations in area 1 might transform the cross-finger orientation disparity of area 3b cells into a common orientation preference map that is then relayed to SII. Another possibility is that these cross-finger tuning discrepancies arise from intrinsic computations within subpopulation of neurons in area 3b. A more provocative explanation is that orientation-tuned MD cells in area 3b receive feedback input from multiple SII neurons that encode different orientation

angles. Cells that integrate inputs from multiple fingers and have cross-finger orientation preferences that differ between 22.5° and 67.5° are advantageous (e.g., less computationally demanding) for representing non-squared objects (e.g., triangular or hexagonal-shaped object). For instance, a population readout that represents a non-squared object could be achieved by sampling from a limited set of MD neurons that have relatively similar orientation tuning preferences in the preferred digit but phased-shifted preferred orientations in the non-preferred digits. In contrast, neural representations of non-squared objects derived from a population with orientation tuning properties similar to those in SII would require readout from a larger set of cells that differ in orientation preferences, thus making the process more computationally expensive. This latter mechanism requires a selective and convoluted combination of cells that have orientation preference disparities between 22.5° and 67.5° across each digit.

It is unclear whether similar cross-finger preference shifts take place in MD cells that encode other types of touch features such as force, texture, and motion. It is possible that these cross-finger preference shifts are limited to ‘‘spatial’’ tactile features such as orientation and curvature because they need to be combined to generate the overall contour of the object (see above). Yet, for tactile motion direction, this cross-finger preference shift does not seem to be an efficient coding strategy. Instead, it seems beneficial that all fingers have a preferred response to the same motion direction in order to provide a coherent representation of motion of the traveling object. Similar predictions are made for MD neurons encoding force and texture. These hypotheses need to be tested in future studies.

Conclusion

The traditional view in the somatosensory system indicates that object perception emerges across cortical stages, with area 3b serving as a ‘‘feature detector’’ cortical relay site.[1] Recent studies push against this framework by showing that neurons in area 3a and 3b integrate inputs from both cutaneous and proprioceptive modalities.[24] Our study further argues against this ‘‘serial model’’ of object perception by demonstrating that area 3b has cells that encode orientation signals across multiple fingers using a coding scheme that may be amenable for representing curved objects. Further, we found higher orientation selectivity in SD vs. MD cells. Based on these observations, we propose two parallel functional pathways in area 3b: (1) a ‘‘*spatial acuity*’’ pathway, comprising SD cells, which is important for providing a detailed representation of particular tactile spatial features, and (2) an ‘‘*object-shape formation*’’ pathway, comprising MD cells, which is integral to the process of generating a neural representation of the 3D contour of tactile objects.

Limitations of the study

We were unable to anatomically confirm the location of our recordings using histological methods. As mentioned earlier, we relied on physiological responses and depth of recordings to restrict analyses to area 3b, an approach that has been used by many single-unit studies in area 3b that have used both neurophysiological and histological methods to verify recordings from area 3b. That said, future non-human primate studies investigating MD RF properties of area 3b cells need to integrate histology and physiology to explicitly confirm the recording locations.

Our findings are also limited in determining how area 3b MD RFs are modulated by concurrent simulation across digits (e.g., modulate non-classical RF properties). Our experimental protocol delivered stimulation to digits 2 through 5 individually. As such, it is unclear how MD stimulation modulates area 3b cells' firing rate properties in the macaque brain. Previous work in owl monkeys showed that co-stimulation of digits is predominantly suppressive in the preferred digit, with maximal suppression occurring when the non-preferred digit is stimulated 30 ms prior to the preferred digit.[26] Whether similar effects occur in rhesus macaques is yet unknown.

STAR☆METHODS

RESOURCE AVAILABILITY

Lead contact: Further information, questions, and requests should be directed to and will be fulfilled by the lead contact, Dr. Manuel Gomez-Ramirez (mgomezra@ur.rochester.edu).

Materials availability: This study did not generate new materials.

Data and code availability: All data reported in this paper will be shared by the lead contact upon request. This paper does not report original code. Any additional information required to reanalyze the data reported in this work paper is available from the lead contact upon request.

EXPERIMENTAL MODEL AND SUBJECT DETAILS

Experiments were conducted in two male rhesus (Macaca mulatta; 8.1–9.7 kg weight) monkeys. Each monkey underwent surgery under anesthesia to implant head restraining posts and recording chambers. Recording chambers (stainless steel, 19 mm diameter) were placed on both hemispheres to target the hand region of somatosensory cortex, centered over the Horsley-Clarke coordinates anterior/posterior = 6, medial/lateral = ±22. All surgical and experimental procedures were approved by the Animal Care and Use Committee of the Johns Hopkins University and conformed to National Institutes of Health and U.S. Department of Agriculture guidelines.

METHOD DETAILS

Animals sat in a comfortable chair with their head restrained, and tested hand in a supinated posture. The fingers on the tested hand were placed comfortably in a hand holder, with digits 2 through 5 secured with cloth tape around the medial pads, and the fingernails secured with a small amount of fixative to a nail holder. A custom-made tactile stimulator device was used to systematically map the RF and orientation tuning properties of cells on the distal pad of D2-D5 (Figure 1). The tactile stimulator was a linear motor mounted on the shaft of a rotating stepper motor (Arsape AM 1020, 10 mm diameter, 15.9 mm length, Faulhaber, Clearwater, Fl.). The oriented bar was 3D printed (Objet Alaris 30U), 10mm long, approximately the width of a monkey's finger, with its short axis equal to 3 mm. A wedge-shaped bar (90°) was used to produce a robust edge sensation of a surface. The motors were attached to an articulated tool holder (Noga Engineering Ltd. Shlomi 22832, Israel) mounted to a micro-positioner (Newport Corp., California) and a magnetic base. The

animal's fingers were slightly spread to avoid the bar contacting multiple digits. The bar was presented for 500 ms, with a ramp time of 20ms, 1mm indented into the skin, and with an orientation between 0° and 157.5° (steps of 22.5°). Each orientation was presented eight times. The interstimulus interval (ISI) was 700 ms.

Animals were trained to perform a visual discrimination task to keep them aroused while they were presented with tactile stimuli. Our experience has been that monkeys engaged in simple discrimination tasks usually result in a more cooperative animal, facilitating longer recording times from individual cells. The visual task began with presentation of a blue square with size of 2.04°. After 400 ms of fixation, two white circles appeared on the left and right of the visual cue (each 2.04° in diameter). The circles had different luminance levels, and the animal was required to make a saccade to the brighter circle. The two visual circles were presented for a maximum of 2000 msec. The inter-trial-interval was 2300 msec. The discrimination difficulty was adapted using an ongoing staircase method based on the animal's performance.[32] The difficulty increased (i.e. the luminance difference decreased, using a logarithmic scale) following three successive correct trials, and decreased after each error. The animal was rewarded with a drop of liquid after every correct response. All visual stimuli were presented on a Samsung SyncMaster 740b 17″ LCD monitor, on a black background with a 60 Hz refresh rate. Eye position was monitored with a PC-60 ViewPoint EyeTracker (Arrington Research - Scottsdale, AZ).

Neurophysiology: Neural activity was recorded from area 3b from four hemispheres (see supplementary material for details on training in each animal). Standard neurophysiological techniques were used to collect the data in all animals.[13,24,32,56,57] Prior to recording, a craniotomy was made in the center of the recording chamber, approximately 3 mm in diameter. Thereafter, the animal was brought in daily to the laboratory (6 days/week), the chamber cover removed, the chamber rinsed with sterile saline, and a positioning stage mounted onto the chamber. A custom-built microdrive system was secured to this positioning stage, containing four separate extracellular microelectrodes (2 to 7MU, Tungsten FHC Inc, Bowdoin, ME) linearly aligned and spaced 584 μm apart. The animal was transferred to the recording room, and the electrodes advanced through the intact dura and cortex. Electrodes were removed, the chamber cleaned, and a small piece of gelfoam with dexamethasone and antibiotic was placed on the dura the end of each recording day. The chamber was filled with sterile saline and sealed, and the animal placed back in its home cage. As recordings progressed, the initial craniotomy was expanded to cover the 3b hand region.

We used similar functional mapping procedures as in previous studies to ensure we recorded single units from area 3b, which resides in the postcentral gyrus.[10,14,18,19,28,29] The central sulcus was determined by the depth and transitions of white and gray matter, as well by the presence of motor responses in anterior electrodes. We positioned the recording array in an anterior-posterior orientation to predominantly cover neural representations from the same digit. It took approximately a week to localize the neural representation of digits 2–5 (D2-D5) of area 3b. After localizing D2-D5 of area 3b, the electrode array was shifted 100 μm on each recording day, on the anterior-posterior axis, to track the postcentral gyrus until

the entire 3b representation of D2-D5 was covered (see Figure S5). We recorded activity from each hemisphere for about 2 months.

Electrodes were positioned to penetrate the brain perpendicularly. Electrodes contacted area 1 (or sometimes area 2), which lie in the surface of the brain. As one descends from the cortical surface through area 1, RFs progress from the distal, to middle, to proximal finger pads, and then to the palmar whorls. When electrodes reach area 3b, RFs proceed back up the finger, transitioning from proximal, to medial, and ultimately to distal pads. This reversed topographical representation between distal and proximal pads is a hallmark of the boundary region between area 3b and 1 (DiCarlo et al., 1998). Thus, we focused our recordings on cells with an RF on the distal pads of D2-D5 because recordings from the proximal pad of area 3b may lead to the inclusion of area 1 cells with an RF over the proximal pad. We selected cells recorded >2mm below the surface of the brain to avoid analyzing cells in area 1 (range = ~2 to ~5mm past the estimated location of electrode contact with dura). Due to technical and logistical challenges, we did not perform histological analyses to anatomically confirm that recordings were made from area 3b. However, we reiterate that we used similar functional mapping procedures as previous experiments that studied response properties of area 3b cells,[14,18,19,24,28,29] and the temporal and topographical properties of our neural recordings are highly consistent with the response properties of area 3b cells.

RF mapping and orientation selectivity: We first isolated single units with an RF on the distal pads of D2 – D5 via manual mapping procedures. Afterward, a custom-made tactile stimulator device was used to deliver tactile stimuli of different orientations to the distal pad of D2-D5. We only analyzed cells where the orientation selectivity and RF mapping procedure was fully conducted in D2-D5 distal pads.

A large fraction of somatosensory cells have inhibited responses to the presentation of a tactile stimulus.[12,13,32,56] Thus, we computed the absolute value of baselined responses to capture the firing rate power elicited by the stimulus regardless of response directionality (i.e., inhibited vs. excited; Equation 1).

$$\widehat{R} = \left| R_{stim} - R_{baseline} \right| \quad \text{(Equation 1)}$$

where $\widehat{R}$ is the absolute value of the difference between the baseline firing rate ($R_{baseline}$) and the firing rate during the stimulus (R_{stim}). We defined the cell's 'preferred' digit as the stimulated digit that evoked the highest $\widehat{R}$. The cell was classified as 'excited' or 'inhibited' depending on whether the post-stimulus response was greater (excited) or lower (inhibited) to the mean activity in the baseline period.

We estimated a neuron's response variability to tactile stimulation in the preferred digit by quantifying the Fano Factor (FF, see Equation 2).

$$FF = \frac{\sigma\left(\widehat{R}\right)^2}{X\left(\widehat{R}\right)}$$

(Equation 2)

where σ and represent the variance and mean across all trials in the digit that evoked the maximal response (i.e., the preferred digit). A value of one, indicates a cell with Poisson distributed responses across digits. A number below one indicates a cell with low variability to tactile stimulation, whereas a value greater than one represents a cell with high response variability to tactile stimulation.

Orientation selectivity for each digit was computed using Equation 3

$$OI = \frac{\sqrt{\left[\sum_{i=1}^{K} \widehat{R}(i) x \sin(2\theta_i)\right]^2 + \left[\sum_{i=1}^{K} \widehat{R}(i) x \cos(2\theta_i)\right]^2}}{\sum_{i=1}^{K} \widehat{R}(i)}$$

(Equation 3)

where $\widehat{R}(i)$ is the average baselined absolute firing rate in response to the bar at orientation Θ_i. We used the average response over the entire stimulus period (onset to 100msec after offset), as it has been shown that orientation selectivity can vary over the stimulus period.[14] Values of the orientation index (OI) range from 0, where a neuron has a uniform response to all orientations, to 1, where the neuron has a non-zero response to only 1 orientation. For each neuron, we determined the statistical significance of OI by randomizing responses across repetitions 5000 times and recalculating OI each time to obtain a distribution of values expected by chance.[58] A separate randomization distribution was calculated for each cell. We defined tuning to be significant when the observed OI value exceeded 95% of the values in the randomized distribution. The preferred orientation was determined as the orientation that elicited the highest response. Circular correlation methods were performed to determine the similarity in orientation tuning preference between preferred and non-preferred digits of MD cells.

Ensuring single unit (SU) isolation: We performed several methods to ensure that recordings across all sessions were obtained from the same cell.[32] Implementing ‘sanity check’ methods for SU identification is critical, as multi-unit recordings may lead to the incorrect assignment of a cell with an MD RF. SUs were isolated using a template-based spike sorter, and only one neuron per electrode was recorded at a time.[59] The shape and timing information of each action potential (AP) was stored, and additional SU isolation analyses were performed offline to ensure that SU activity was well isolated. First, spikes occurring within 3msec of one another were excluded, as it would be unlikely to observe such spikes from the same neuron. Next, the shape of the AP was subjected to principal component analysis (PCA), and shapes that were more than three standard deviations away from the center of mass of the two most principal components (using the normalized Euclidean distance method) were deleted. Next, the experimenter visually inspected each

block of trials, and manually deleted AP shapes that were deemed outliers. Finally, we sorted the mean firing rate of a cell across trials within one protocol, and fitted the sorted firing rates with power function. Trials from the tail ends were deleted until the fit produced a non-significant fit ($p > 0.05$). Since the experimental conditions were uniformly randomized, a negative or positive slope of the sorted trials would be indicative of cell loss or inclusion of APs from nearby cells, respectively. Cells with less than 30 trials were not included in the analyses. Cells with less than 30 trials were not included in the analyses. As mentioned previously, we only analyzed cells with an RF on the distal pads and from depth recordings > 2mm below the surface of the brain. This selection criteria was performed to avoid including cells from area 1, which have been shown to have MD RFs. Our analyses led to 477 SUs from the hand regions of area 3b, of which 223 neurons were recorded from two hemispheres in animal MR4358M, and 254 were recoded from two hemispheres in animal 43V.

Determining the temporal evolution of neural responses: We performed a temporal clustering analysis to determine whether the digit RF size of cells increased across time or emerged within similar time frames. On each trial, we epoched the data between stimulus onset to 160ms after stimulus onset (to ensure that 'Off' responses were included in the analyses), and divided the epoch into 20ms bins. For each bin, we determined whether the average response was significantly different than baseline (using Wilcoxon rank-sum test, $p < 0.05$). The baseline activity was computed as the average response between −450 and −250msec, relative to stimulus onset. If a cell had two consecutive bins with a significant response in the same direction with respect to baseline (two consecutive negative or positive bins), we considered that cell to have a significant response on that digit.[24]

QUANTIFICATION AND STATISTICAL ANALYSIS

Details of data processing and statistical analyses can be found in the Methods details and the Results sections. The data were processed using custom-made code in MATLAB. Statistical analyses were conducted using non-parametric statistics (e.g., bootstrapping, Wilcoxson, Kruskall-Wallis tests, etc.). Details of the statistical tests are described in the Results section. The number of observations in the analyses represent the number of cells, except for the analyses conducted in each cell to determine whether a digit has a significant response to tactile stimulation. In these single-cell analyses n represents the number of tactile stimuli delivered. Unless, otherwise noted, error bars in the figures represent Standard Error of the Mean (SEM).

Supplementary Material

Refer to Web version on PubMed Central for supplementary material.

ACKNOWLEDGMENTS

We would like to express our sincere gratitude to Justin Killebrew, William Nash, and William Quinlan (The Bills) from Johns Hopkins University for their invaluable technical assistance on the project. In addition, we would like to thank Drs. Marc Schieber and Greg DeAngelis from the University of Rochester for their insightful comments on the manuscript, and Kristjana Hysaj for helping to train and take care of the animals. This work was funded by NIH NINDS grants NS114191 (M.G.R.), NS073309 (N.K.T.), NS034086 (S.S.H.), NS018787 (S.S.H.), and NS018787–26S1 (S.S.H.).

REFERENCES

1. Hsiao S (2008). Central mechanisms of tactile shape perception. Curr. Opin. Neurobiol 18, 418–424. [PubMed: 18809491]
2. Mountcastle VB (2005). The Sensory Hand: Neural Mechanisms of Somatic Sensation (Harvard University Press).
3. Hsiao SS, and Gomez-Ramirez M (2013). Neural mechanisms of tactile perception. In Handbook of Psychology: Behavioral Neuroscience (John Wiley & Sons Ltd), pp. 206–239. Vol. 3. 2nd ed.
4. Sur M (1980). Receptive fields of neurons in areas 3b and 1 of somatosensory cortex in monkeys. Brain Res 198, 465–471. [PubMed: 6250672]
5. Pons TP, Wall JT, Garraghty PE, Cusick CG, and Kaas JH (1987). Consistent features of the representation of the hand in area 3b of macaque monkeys. Somatosens. Res 4, 309–331. [PubMed: 3589287]
6. Iwamura Y, Tanaka M, Sakamoto M, and Hikosaka O (1983). Functional subdivisions representing different regions in area 3 of the first somatosensory cortex of the conscious monkey. Exp. Brain Res 51, 315–326.
7. Iwamura Y, Iriki A, and Tanaka M (1994). Bilateral hand representation in the postcentral somatosensory cortex. Nature 369, 554–556. [PubMed: 8202155]
8. Jenkins WM, Merzenich MM, Ochs MT, Allard T, and Guíc-Robles E (1990). Functional reorganization of primary somatosensory cortex in adult owl monkeys after behaviorally controlled tactile stimulation. J. Neurophysiol 63, 82–104. [PubMed: 2299388]
9. Wang X, Merzenich MM, Sameshima K, and Jenkins WM (1995). Remodelling of hand representation in adult cortex determined by timing of tactile stimulation. Nature 378, 71–75. [PubMed: 7477291]
10. DiCarlo JJ, Johnson KO, and Hsiao SS (1998). Structure of receptive fields in area 3b of primary somatosensory cortex in the alert monkey. J. Neurosci 18, 2626–2645. [PubMed: 9502821]
11. Sripati AP, Yoshioka T, Denchev P, Hsiao SS, and Johnson KO (2006). Spatiotemporal receptive fields of peripheral afferents and cortical area 3b and 1 neurons in the primate somatosensory system. J. Neurosci 26, 2101–2114. [PubMed: 16481443]
12. Fitzgerald PJ, Lane JW, Thakur PH, and Hsiao SS (2004). Receptive field properties of the macaque second somatosensory cortex: evidence for multiple functional representations. J. Neurosci 24, 11193–11204. [PubMed: 15590936]
13. Thakur PH, Fitzgerald PJ, Lane JW, and Hsiao SS (2006). Receptive field properties of the macaque second somatosensory cortex: nonlinear mechanisms underlying the representation of orientation within a finger pad. J. Neurosci 26, 13567–13575. [PubMed: 17192440]
14. Bensmaia SJ, Denchev PV, Dammann JF, Craig JC, and Hsiao SS (2008). The representation of stimulus orientation in the early stages of somatosensory processing. J. Neurosci 28, 776–786. [PubMed: 18199777]
15. Ageranioti-Bélanger SA, and Chapman CE (1992). Discharge properties of neurones in the hand area of primary somatosensory cortex in monkeys in relation to the performance of an active tactile discrimination task. Areas 3b and 1. Exp. Brain Res 91, 207–228. [PubMed: 1459224]
16. Costanzo RM, and Gardner EP (1980). A quantitative analysis of responses of direction-sensitive neurons in somatosensory cortex of awake monkeys. J. Neurophysiol 43, 1319–1341. [PubMed: 6768849]
17. Gardner EP, Ro JY, Debowy D, and Ghosh S (1999). Facilitation of neuronal activity in somatosensory and posterior parietal cortex during prehension. Exp. Brain Res 127, 329–354. [PubMed: 10480270]
18. Pei Y-C, Denchev PV, Hsiao SS, Craig JC, and Bensmaia SJ (2009). Convergence of submodality-specific input onto neurons in primary somatosensory cortex. J. Neurophysiol 102, 1843–1853. [PubMed: 19535484]
19. Pei Y-C, Hsiao SS, Craig JC, and Bensmaia SJ (2010). Shape invariant coding of motion direction in somatosensory cortex. PLoS Biol 8, e1000305. [PubMed: 20126380]

20. Sur M, Wall JT, and Kaas JH (1984). Modular distribution of neurons with slowly adapting and rapidly adapting responses in area 3b of somatosensory cortex in monkeys. J. Neurophysiol 51, 724–744. [PubMed: 6716121]
21. Sur M, Garraghty PE, and Bruce CJ (1985). Somatosensory cortex in macaque monkeys: laminar differences in receptive field size in areas 3b and 1. Brain Res 342, 391–395. [PubMed: 4041845]
22. Warren S, Hamalainen HA, and Gardner EP (1986). Objective classification of motion- and direction-sensitive neurons in primary somatosensory cortex of awake monkeys. J. Neurophysiol 56, 598–622. [PubMed: 3783213]
23. Sur M, Merzenich MM, and Kaas JH (1980). Magnification, receptivefield area, and 'hypercolumn' size in areas 3b and 1 of somatosensory cortex in owl monkeys. J. Neurophysiol 44, 295–311. [PubMed: 7411189]
24. Kim SS, Gomez-Ramirez M, Thakur PH, and Hsiao SS (2015). Multimodal interactions between proprioceptive and cutaneous signals in primary somatosensory cortex. Neuron 86, 555–566. [PubMed: 25864632]
25. Sur M, Wall JT, and Kaas JH (1981). Modular segregation of functional cell classes within the postcentral somatosensory cortex of monkeys. Science 212, 1059–1061. 10.1126/science.7233199. [PubMed: 7233199]
26. Reed JL, Qi HX, Zhou Z, Bernard MR, Burish MJ, Bonds AB, and Kaas JH (2010). Response properties of neurons in primary somatosensory cortex of owl monkeys reflect widespread spatiotemporal integration. J. Neurophysiol 103, 2139–2157. [PubMed: 20164400]
27. Lazar L, Chand P, Rajan R, Mohammed H, and Jain N (2022). Somatosensory Cortex of Macaque Monkeys Is Designed for Opposable Thumb 10.1101/2020.08.31.261115.
28. Pei Y-C, Hsiao SS, Craig JC, and Bensmaia SJ (2011). Neural mechanisms of tactile motion integration in somatosensory cortex. Neuron 69, 536–547. [PubMed: 21315263]
29. Thakur PH, Fitzgerald PJ, and Hsiao SS (2012). Second-order receptive fields reveal multidigit interactions in area 3b of the macaque monkey. J. Neurophysiol 108, 243–262. [PubMed: 22457468]
30. Bourgeon S, Dépeault A, Meftah E-M, and Chapman CE (2016). Tactile texture signals in primate primary somatosensory cortex and their relation to subjective roughness intensity. J. Neurophysiol 115, 1767–1785. [PubMed: 26763776]
31. Qi H-X, Reed JL, Franca JG, Jain N, Kajikawa Y, and Kaas JH (2016). Chronic recordings reveal tactile stimuli can suppress spontaneous activity of neurons in somatosensory cortex of awake and anesthetized primates. J. Neurophysiol 115, 2105–2123. [PubMed: 26912593]
32. Gomez-Ramirez M, Trzcinski NK, Mihalas S, Niebur E, and Hsiao SS (2014). Temporal correlation mechanisms and their role in feature selection: a single-unit study in primate somatosensory cortex. PLoS Biol 12, e1002004. [PubMed: 25423284]
33. Reed JL, Qi HX, Pouget P, Burish MJ, Bonds AB, and Kaas JH (2010). Modular processing in the hand representation of primate primary somatosensory cortex coexists with widespread activation. J. Neurophysiol 104, 3136–3145. [PubMed: 20926605]
34. Shin H, and Moore CI (2019). Persistent gamma spiking in SI nonsensory fast spiking cells predicts perceptual success. Neuron 103, 1150–1163.e5. [PubMed: 31327663]
35. Tabot GA, Dammann JF, Berg JA, Tenore FV, Boback JL, Vogelstein RJ, and Bensmaia SJ (2013). Restoring the sense of touch with a prosthetic hand through a brain interface. Proc. Natl. Acad. Sci. USA 110, 18279–18284. [PubMed: 24127595]
36. Friedman RM, Chen LM, and Roe AW (2008). Responses of areas 3b and 1 in anesthetized squirrel monkeys to single- and dual-site stimulation of the digits. J. Neurophysiol 100, 3185–3196. [PubMed: 18922955]
37. Hildebrandt KJ, Sahani M, and Linden JF (2017). The impact of anesthetic state on spike-sorting success in the cortex: a comparison of ketamine and urethane anesthesia. Front. Neural Circuits 11, 95. [PubMed: 29238293]
38. Krom AJ, Marmelshtein A, Gelbard-Sagiv H, Tankus A, Hayat H, Hayat D, Matot I, Strauss I, Fahoum F, Soehle M, et al. (2020). Anesthesia-induced loss of consciousness disrupts auditory responses beyond primary cortex. Proc. Natl. Acad. Sci. USA 117, 11770–11780. [PubMed: 32398367]

39. Sorrenti V, Cecchetto C, Maschietto M, Fortinguerra S, Buriani A, and Vassanelli S (2021). Understanding the effects of anesthesia on cortical electrophysiological recordings: a scoping review. Int. J. Mol. Sci 22, 1286. [PubMed: 33525470]
40. Meinecke DL, and Peters A (1987). GABA immunoreactive neurons in rat visual cortex. J. Comp. Neurol 261, 388–404. [PubMed: 3301920]
41. Gabernet L, Jadhav SP, Feldman DE, Carandini M, and Scanziani M (2005). Somatosensory integration controlled by dynamic thalamocortical feed-forward inhibition. Neuron 48, 315–327. [PubMed: 16242411]
42. Cruikshank SJ, Lewis TJ, and Connors BW (2007). Synaptic basis for intense thalamocortical activation of feedforward inhibitory cells in neocortex. Nat. Neurosci 10, 462–468. [PubMed: 17334362]
43. Porter JT, Johnson CK, and Agmon A (2001). Diverse types of inter-neurons generate thalamus-evoked feedforward inhibition in the mouse barrel cortex. J. Neurosci 21, 2699–2710. [PubMed: 11306623]
44. Bruno RM, and Simons DJ (2002). Feedforward mechanisms of excitatory and inhibitory cortical receptive fields. J. Neurosci 22, 10966–10975. [PubMed: 12486192]
45. Isaacson JS, and Scanziani M (2011). How inhibition shapes cortical activity. Neuron 72, 231–243. [PubMed: 22017986]
46. Minamisawa G, Kwon SE, Chevée M, Brown SP, and O'Connor DH (2018). A non-canonical feedback circuit for rapid interactions between somatosensory cortices. Cell Rep 23, 2718–2731.e6. [PubMed: 29847801]
47. Liao C-C, and Yen C-T (2008). Functional connectivity of the secondary somatosensory cortex of the rat. Anat. Rec 291, 960–973.
48. Ashaber M, Pálfi E, Friedman RM, Palmer C, Jákli B, Chen LM, Kántor O, Roe AW, and Négyessy L (2014). Connectivity of somatosensory cortical area 1 forms an anatomical substrate for the emergence of multifinger receptive fields and complex feature selectivity in the squirrel monkey (Saimiri sciureus). J. Comp. Neurol 522, 1769–1785. [PubMed: 24214200]
49. Liao C-C, Gharbawie OA, Qi H, and Kaas JH (2013). Cortical connections to single digit representations in area 3b of somatosensory cortex in squirrel monkeys and prosimian galagos. J. Comp. Neurol 521, 3768–3790. [PubMed: 23749740]
50. Pálfi E, Zalányi L, Ashaber M, Palmer C, Kántor O, Roe AW, Friedman RM, and Négyessy L (2018). Connectivity of neuronal populations within and between areas of primate somatosensory cortex. Brain Struct. Funct 223, 2949–2971. [PubMed: 29725759]
51. Lederman SJ, and Klatzky RL (1987). Hand movements: a window into haptic object recognition. Cogn. Psychol 19, 342–368. [PubMed: 3608405]
52. Johansson RS, and Vallbo AB (1979). Tactile sensibility in the human hand: relative and absolute densities of four types of mechanoreceptive units in glabrous skin. J. Physiol 286, 283–300. [PubMed: 439026]
53. Fitzgerald PJ, Lane JW, Thakur PH, and Hsiao SS (2006). Receptive field properties of the macaque second somatosensory cortex: representation of orientation on different finger pads. J. Neurosci 26, 6473–6484. [PubMed: 16775135]
54. Jones EG, and Powell TP (1969). Connexions of the somatic sensory cortex of the rhesus monkey. I. Ipsilateral cortical connexions. Brain 92, 477–502. [PubMed: 4979846]
55. Jones EG, and Powell TP (1969). Connexions of the somatic sensory cortex of the rhesus monkey. II. Contralateral cortical connexions. Brain 92, 717–730. [PubMed: 4983244]
56. Ray S, Hsiao SS, Crone NE, Franaszczuk PJ, and Niebur E (2008). Effect of stimulus intensity on the spike–local field potential relationship in the secondary somatosensory cortex. J. Neurosci 28, 7334–7343. [PubMed: 18632937]
57. Steinmetz PN, Roy A, Fitzgerald PJ, Hsiao SS, Johnson KO, and Niebur E (2000). Attention modulates synchronized neuronal firing in primate somatosensory cortex. Nature 404, 187–190. [PubMed: 10724171]
58. Yau JM, Pasupathy A, Fitzgerald PJ, Hsiao SS, and Connor CE (2009). Analogous intermediate shape coding in vision and touch. Proc. Natl. Acad. Sci. USA 106, 16457–16462. [PubMed: 19805320]

59. Thakur PH, Lu H, Hsiao SS, and Johnson KO (2007). Automated optimal detection and classification of neural action potentials in extra-cellular recordings. J. Neurosci. Methods 162, 364–376. [PubMed: 17353053]

Highlights

- Area 3b cells have receptive fields that span multiple fingers
- Response latency is faster in cells with a multi- vs. single-finger receptive field
- Area 3b cells' receptive field size increases as a function of time
- Area 3b cells' orientation preference is systematically phase-shifted across fingers

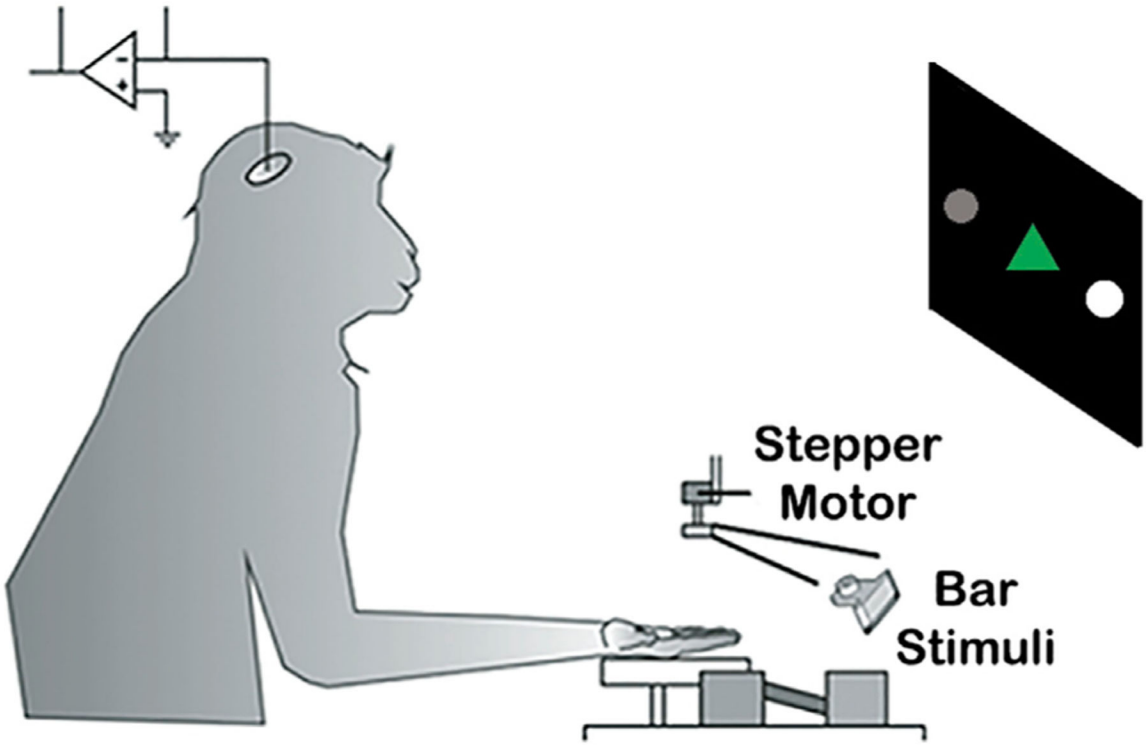

Figure 1. Experimental setup

Animals set in a custom-made chair with their hand supinated and secured. Bars with different orientations were systematically delivered to digits 2–5 while animals were engaged in a visual contrast discrimination task. Animals were trained to fixate on a green triangle and saccade to the flanking circle with highest brightness. After animals were fully trained on the visual task, we recorded single-unit activity from the distal representation of area 3b.

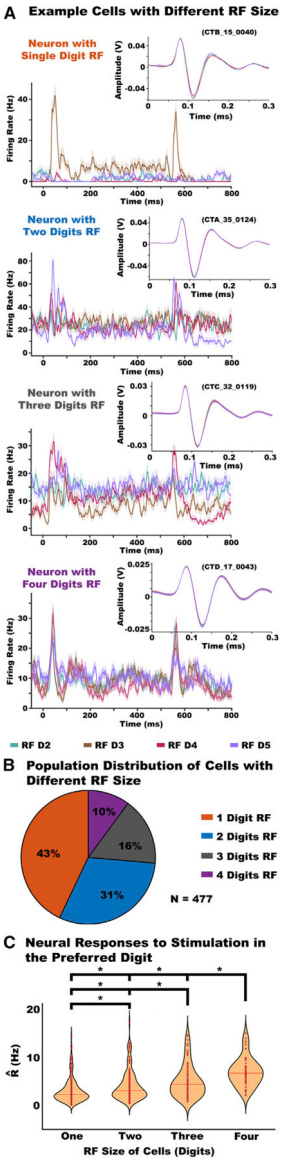

Figure 2. Majority of cells in area 3b have RFs spanning multiple digits

(A) Examples neurons from an RF spanning one (top row), two (second row), three (third row), or four (bottom row) digits. The insets in each graph show action potential waveforms recorded to each stimulated digit.

(B) RF size distribution across the recorded population. Most cells had an RF covering two or more digits (~57% of cells). However, cells with an SD had the largest incidence (~43%), whereas cells with a four-digit RF had the lowest incidence (~10%).

(C) Firing rates to stimulation on the preferred digit increased as a function of cells' RF size. The graph shows violin plots of the normalized firing rate (R) distribution for each RF size condition. Each dot represents a cell's mean R. *$p < 0.01$.

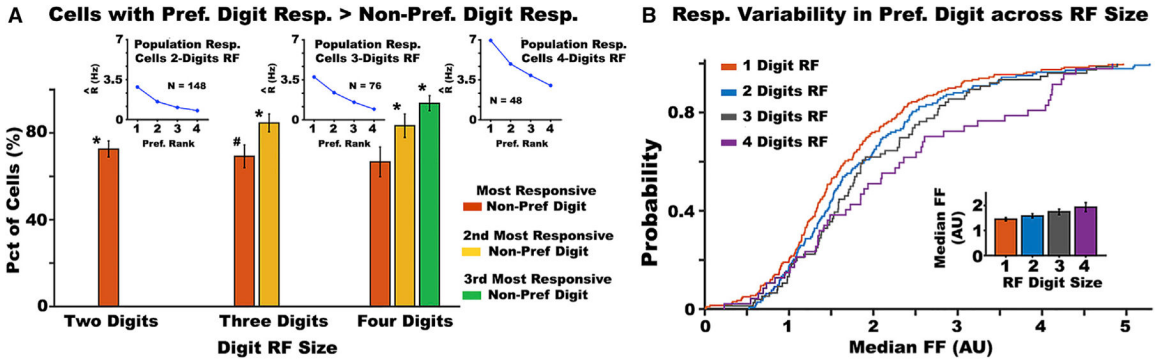

Figure 3. Response variability in preferred digits increases with RF digit size

(A) Percentage of cells with a particular digit eliciting a higher response compared with remaining digits. Differences in response magnitude between the preferred and non-preferred digits increased as a function of RF size. We also found a slight decrease in percentage of cells with a unique preferred digit as a function of digit RF size (~73% of two-digit MD cells; ~69% of three-digit MD cells, and ~67% of four-digit MD cells). The inset represents the population response (average activity across recorded cells) to tactile stimulation to each digit for cells with two digits (left inset), three digits (center inset), and four digits (right inset).

(B) Cumulative distribution of the Fano factor response (variance/mean) to stimulation on the preferred digit across cells with difference digit RF size. The data show a systematic shift in the cumulative distribution across RF size, with four-digit RF cells having the largest Fano factor value. The inset shows the median Fano factor value across RF digit size. These data show higher response variability to tactile stimulation on the preferred digit as a function of cells' RF digit size. *$p < 0.05$; #$p < 0.1$. Error bars represent standard error of the mean.

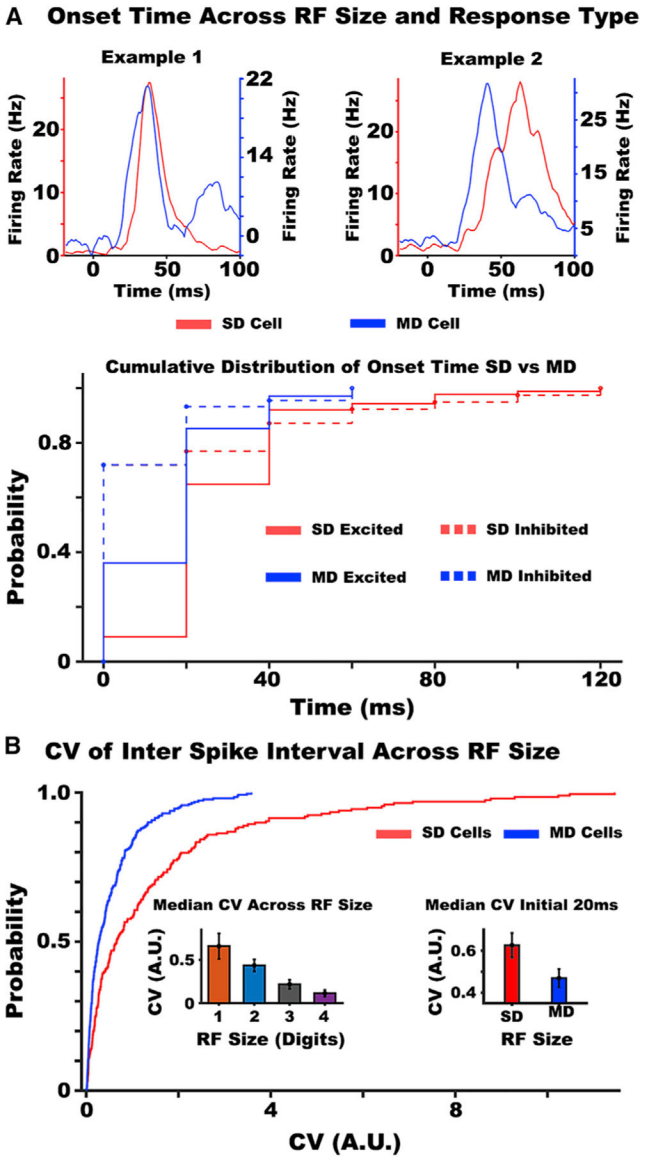

Figure 4. Neural responses have faster onset and are more precise in MD cells

(A) The top graph shows the instantaneous firing rate on the preferred digit of four neurons with excited responses (two in the left panel, two in the right panel) with an SD RF (red trace) and an MD RF (blue trace). Note that the firing rate axes for SD and MD are plotted on the left and right axes, respectively. The lower panel shows the cumulative distribution of onset time for the preferred digit on SD (red traces) and MD (blue traces) cells with excited (solid trace) and inhibited (dashed trace) initial responses. The earliest activations were largely from cells with a response below baseline (i.e., inhibited).

(B) Cumulative distribution of the coefficient of variation (CV) of the inter-spike interval (ISI). The CV of the ISI was lower (i.e., more regular) for MD vs. SD cells. The left shows the median CV of the ISI decreasing as a function of RF size. The right inset shows the median CV of the ISI in MD (blue bar) and SD (red bar) cells with a significant response

during the initial 20 ms relative to stimulus onset. Error bars represent standard error of the mean.

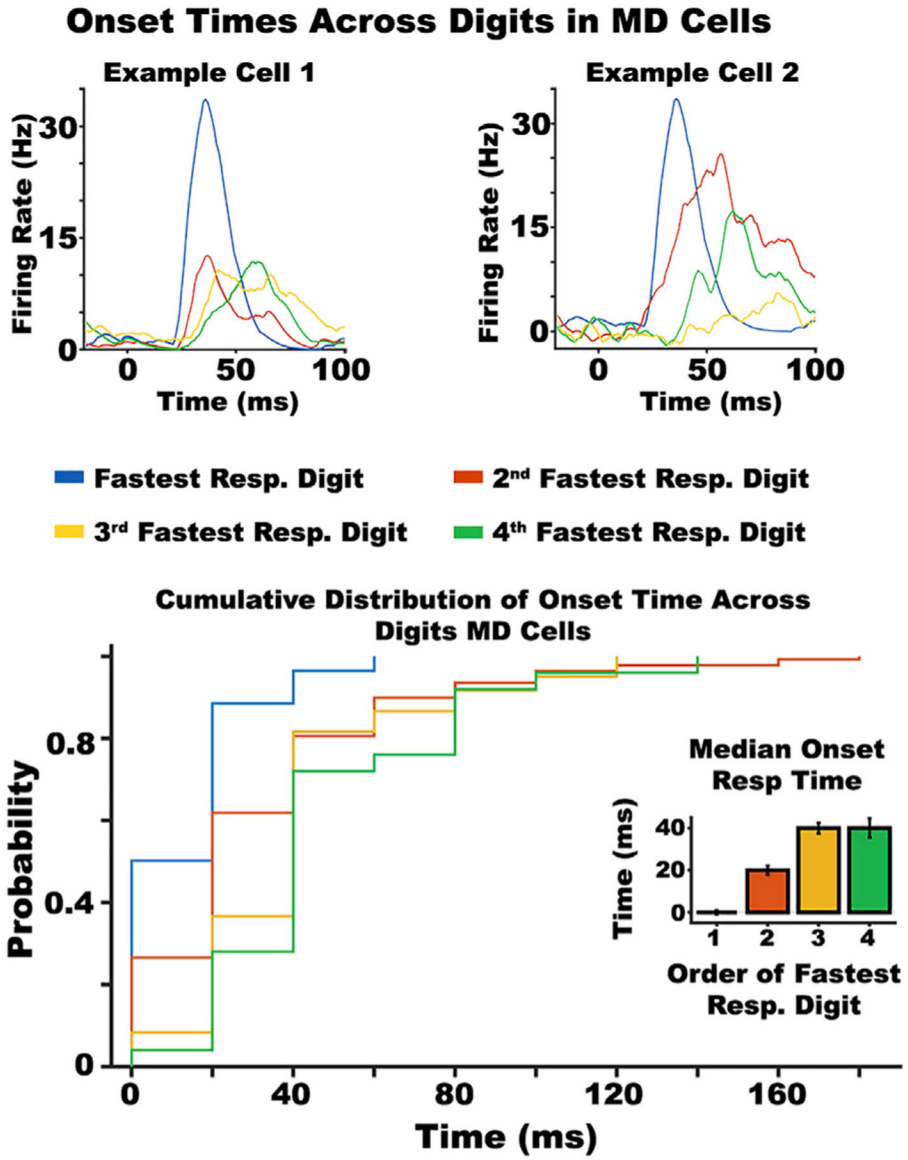

Figure 5. The digit size RF of cells increases across time

The top graphs show examples of neural responses to tactile stimulation on each digit of a cell with an RF spanning four digits. The lower panel shows the cumulative distribution of onset time for each responsive digit across MD cells. The graph shows a systematic shift in response onset times across responsive digits. The inset in the cumulative distribution shows the median response onset time for each responsive digit of MD cells. Error bars represent standard error of the mean.

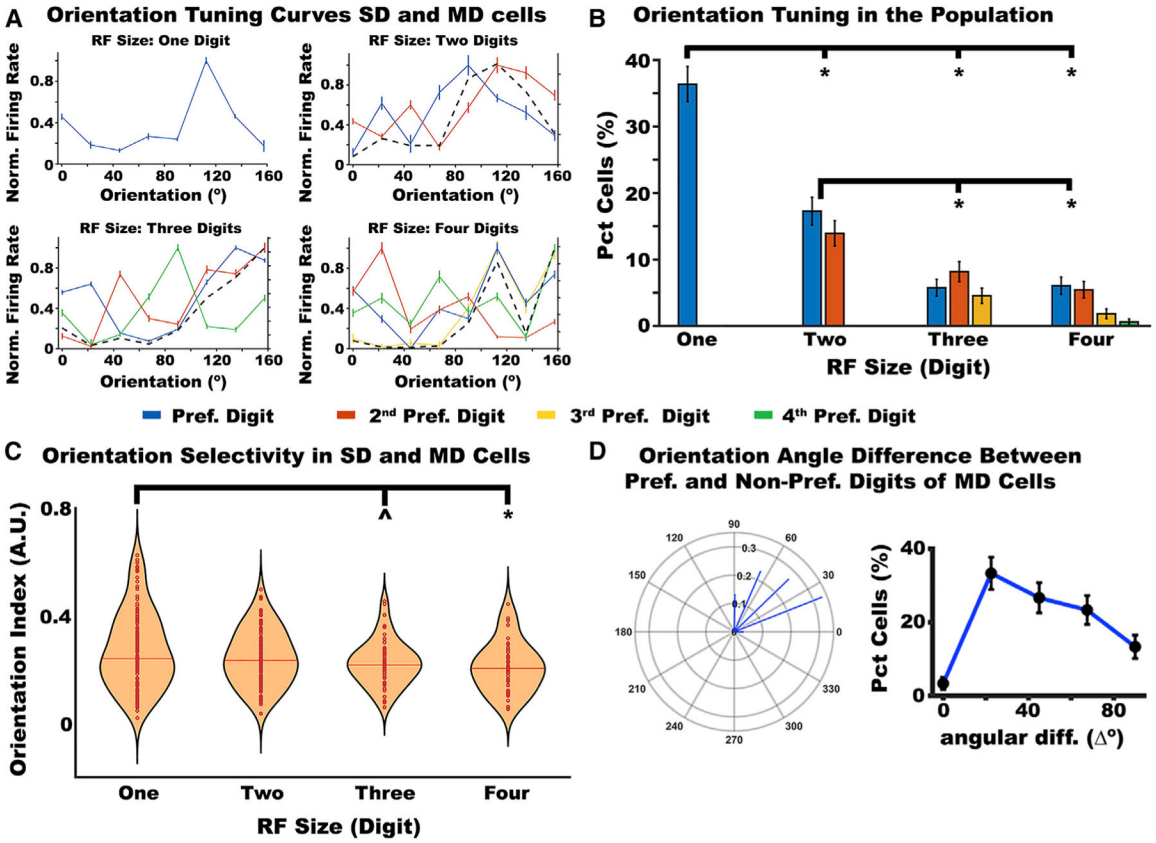

Figure 6. Orientation tuning properties of SD and MD cells

(A) Example orientation tuning curves in cells with one digit (top-left graph), two digits (top-right graph), three digits (bottom-left graph), and four digits RF (bottom-right graph). The dashed black line in MD cells shows the average product of the tuning functions between preferred and non-preferred digits.

(B) The percentage of orientation-tuned cells with a one-, two-, three-, or four-digit RF. The graph indicates that orientation tuning was more prevalent in the preferred digit of cells with an SD vs. MD RF.

(C) Orientation index (OI) in the preferred digit of cells with a one-, two-, three-, or four-digit RF. The data revealed greater orientation selectivity in SD vs. MD cells.

(D) The left panel shows a polar plot of the difference in the preferred angle between preferred and non-preferred digits of orientation-tuned MD cells. Each line represents the length of the difference vector between preferred and non-preferred digits. The right panel shows the percentage of cells with an angular difference between 0° and 90°. Most MD cells have a preferred angle difference between preferred and non-preferred digits of 22.5°. *$p < 0.01$; ^$p = 0.05$. Error bars represent standard error of the mean.

KEY RESOURCES TABLE

Reagent/Resource	Source	Identifier
Experimental models Organisms/strains		
Rhesus non-human primate (*Macaca mulatta*)	Through Johns Hopkins University Research Animal Resources	https://researchanimalresources.jhu.edu/
Software and algorithms		
MATLAB	MathWorks	https://www.mathworks.com/